Progress In Electromagnetics Research C, Vol. 9, 155–169, 2009

WIDE RANGE OF ELECTROSTATIC ACTUATION MEMS FPOTF

N. H. Ngajikin, N. M. Kassim, and A. B. Mohammad

Photonic Technology Centre, Faculty of Electrical Engineering
Universiti Teknologi Malaysia
UTM Skudai, Johor 81310, Malaysia

G. Witjaksono

MIMOS Berhad, Taman Teknologi Malaysia
Kuala Lumpur 57000, Malaysia

Abstract—By employing Microelectromechanical system (MEMS) technology, Fabry-Perot Optical Tunable Filter (FPOTF) with hybrid tuning mechanism, varying d and altering incident angle is presented. The proposed structure consists of a floating dual membrane FPOTF with capability to be tuned at different light incident angles. Three electrostatic cavities have been designed to perform this task independently. This technique is capable to increase the tuning range up to 2/3 of capacitance gap with additional doubly range of incident angle. Optic, mechanic and electrostatic analysis of the proposed structure has been validated by simulation. Analysis in optical performance shows the tuning range enhancement is about 1.92% for $\pm 2^\circ$ mirror tilting at 6° initial angle compared to conventional dual beam MEMS FPOTF. This analysis validates the principle of hybrid tuning method.

1. INTRODUCTION

Due to pull-in voltage phenomena, electrostatic actuation can only offer a small beam deflection which is about 1/3 of capacitance gap [1]. This limitation leads to a low tuning range of electrostatic actuation MEMS FPOTF. Designing a MEMS FPOTF with large length of cavity will increase the wavelength range. This option, however, is limited by fabrication technology where it is a challenge to have a thick gap in optical cavity. Furthermore, increasing the gap size will increase the

Corresponding author: N. H. Ngajikin (nhafizah@fke.utm.my).

operating voltage. Instead of raising the capacitance gap, this paper proposed an alternative, which is hybrid tuning method to improve MEMS FPOTF tuning range.

In review, two mechanisms, either varying length of cavity or adjusting light incident angle, were realized. Most of the inventions is by varying length of cavity using electrostatic actuation [2–31]. As afore mentioned, this type of actuator has limitation in pull in voltage. However, some application with wide spectrum bandwidth requires FPOTF with higher tuning range. Coarse Wavelength Division Multiplexing (CWDM) application, for example, requires at least 360 nm wavelength range.

Two techniques have been proposed previously to enhance the tuning range. The first one is by Verghese [8] using dual membrane MEMS FPOTF. Since both of the mirror holders are movable, the tuning range is doubled to 2/3 capacitance gap. Secondly, Milne et al. [16] used doubly supported beam to reduce strain stiffening to increase the tuning range. The tuning range also can be increased up to 2/3 of capacitance gap. Another wavelength tuning mechanism for FPOTF that had been realized using MEMS technology is shifting the incident angle by mirror tilting. Output spectrum of the MEMS FPOTF with only one mirror tilted consists of more than one mode. This is applicable to multiplexing and channel monitoring application. Besides that, mirror tilting can also enhance filter finesse. Chang and Juan [7] used this technique to adjust mirror flatness in order to have MEMS FPOTF with high finesse.

Hybrid tuning method that has been proposed in this paper will improve tuning range of MEMS FPOTF with electrostatic actuation. The following section will discuss design, working principle and result analysis of this novel structure.

2. MEMS FLOATING FPOTF (f-FPOTF) CONFIGURATION

A novel MEMS floating Fabry-Perot Optical Tunable Filter (f-FPOTF) is proposed to enlarge the tuning range of conventional MEMS FPOTF with electrostatic actuation. This MEMS f-FPOTF has capabilities of varying length of optical cavity and tilting the whole floating cavity at one time. These features not only enlarge the tuning range, but also have capabilities to improve the filter finesse. Equation (1) gives the mathematical expression of FPOTF transmittivity [32].

$$I_t = I_0 \left[1 - \frac{A}{1-R}\right]^2 \left[\frac{1}{1 + M\sin^2(\phi/2)}\right] \tag{1}$$

where $M = \frac{4R}{(1-R^2)}$ and $\phi = 2n_2 dk\cos\theta$. I_0 is the input light; A is the absorption in optical cavity; R is mirror reflectivity; k is propagation constant. This equation shows that the operating wavelength of FPOTF can be altered by either adjusting length of cavity, d, tilting the mirror or by varying the refractive index, n_2 of material inside the optical cavity. Since f-FPOTF combined both tuning, adjusting d and mirror tilting, analysis is done to study the relationship among these three tuning variables with operating wavelength, λ using Equation (2) [42].

$$\lambda = \frac{2n_2 d}{m}\sqrt{1-\left(\frac{\sin\theta}{n_2}\right)} \tag{2}$$

m is the mode number inside the cavity. Let's say that the filter needs to be tuned within CWDM wavelength region (18 operating channels distributed in between 1270 nm to 1610 nm wavelength). Relationship among d, optimal initial angle, θ_o° and range of tuning angle, $\Delta\theta^\circ$ is plotted in Figure 1. Higher initial incident angle contributes to a lower range of tuning angle. However, the range of tuning angle, $\Delta\theta^\circ$, also can be decreased by the increment of d as shown in this graph. Suitable selection of initial angle, θ_i, and initial length of cavity, d_i, will contribute to design that has a large wavelength range with optimal configuration.

In general, tilting FPOTF mirror will broaden the full width half maximum (FWHM) of this filter. This limitation, however, depends on FWHM value of the proposed application.

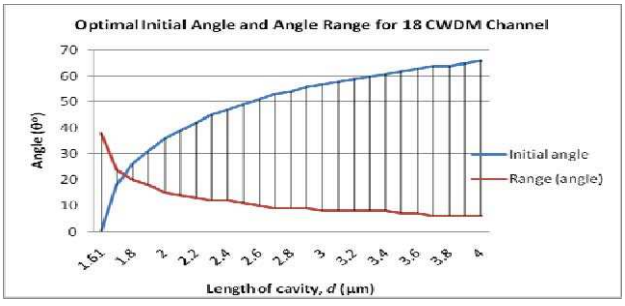

Figure 1. Optimal initial angle, θ_i and range of tuning angle, $\Delta\theta^\circ$ for different value of d.

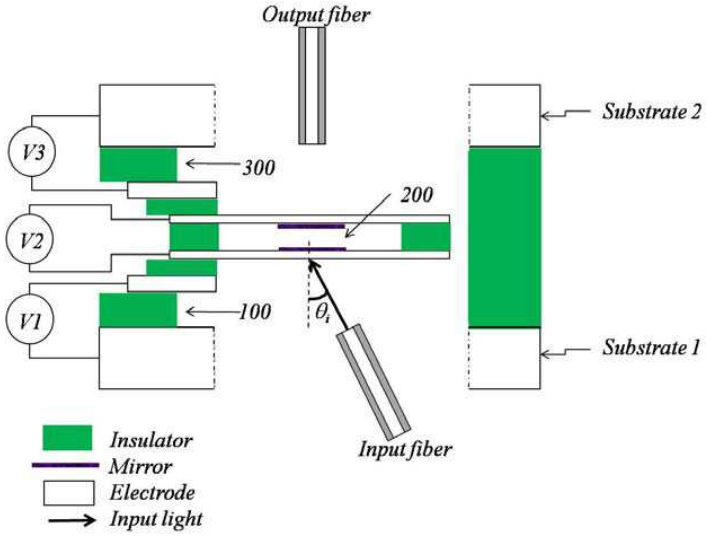

Figure 2. Working principle: Cross-section view of MEMS f-FPOTF.

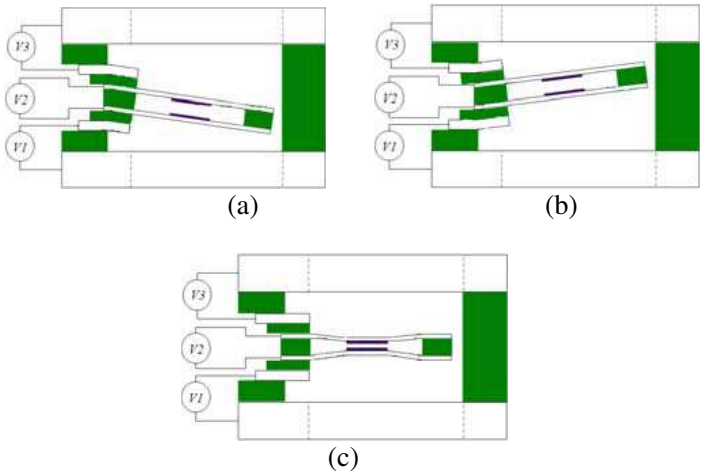

Figure 3. Electrostatic cavity of MEMS f-FPOTF.

2.1. Working Principle

2-dimensional structure of MEMS f-FPOTF is visualized in Figure 2. As afore mentioned, it consists of three electrostatic cavities controlled by 3 independent voltages, which are V_1, V_2 and V_3. V_2 controls the length of cavity, d, while V_1 and V_3 adjust the light incident angle by

activating one of the electrostatic actuator at one time.

Assuming input fiber is located at θ_i° from normal line of FPOTF mirror support. Part 100 which is the first electrostatic cavity will increase light incident angle from the initial position. In oppose, part 300 will decrease the light incident angle. Both of these movements are visualized in Figure 3(a) and Figure 3(b). These features provide wider tuning angle since the floating cavity has potential to deflect both ways, up and down.

Floating Fabry-Perot optical cavity in this filter is labeled as 200 in Figure 2. This is an electrostatic cavity with dual beam actuator. Deflection of dual beam will bring both mirrors closer to each other,

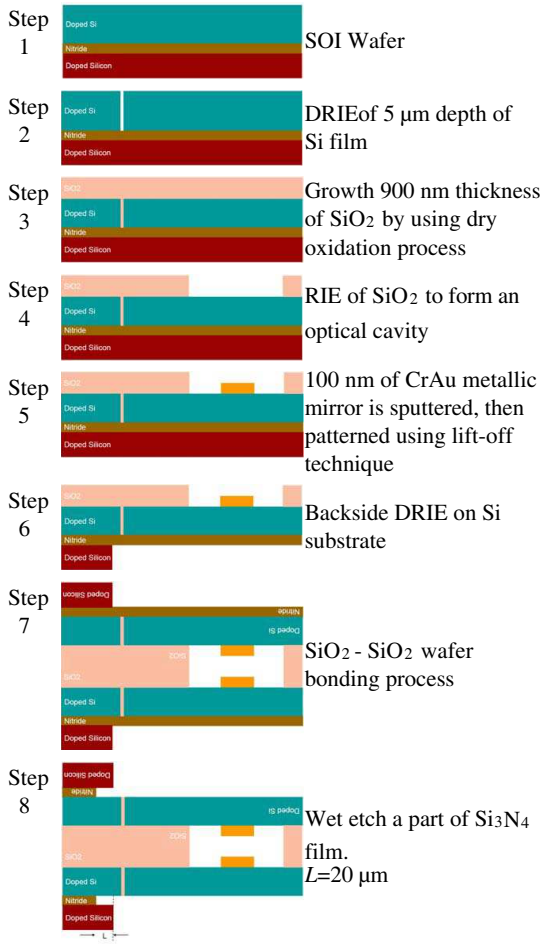

Figure 4. MEMS f-FPOTF fabrication process flow.

hence varying the length of cavity, d. Illustration of this movement is shown in Figure 3(c).

2.2. Structure

Understanding the whole fabrication process flow will determine the suitable mechanic analysis approach for this structure. In this analysis, SOI wafer is used to simplify the whole fabrication process. Device layer on SOI wafer is etched in order to have two separated beams, BEAM1 and BEAM2. The objective of this separation is to achieve dual beam actuation, BEAM1 for controlling angle and BEAM2 for varying length of cavity. SiO_2 film then is grown on top of this wafer to isolate these two beams and also works as a spacer in Fabry-Perot (FP) cavity. Next, the CrAu metallic thin film is sputtered and patterned to be a FP mirror. Both metallic and Distributed Bragg Reflector (DBR) mirror can be applied. However, metallic mirror is chosen due to its simplicity in fabrication yet limited the initial angle. Then, backside Deep Reactive Ion Etch (DRIE), wafer bonding and Nitride etch are performed step by step to shape this proposed filter. Figure 4 illustrates the fabrication process flow.

Layout and cross-section of the simulated structure are given in Figure 5 and Figure 6 respectively. Insulator between BEAM1 and BEAM2 is not visualized in layout view since the dimension is very small compared to other features in this design. Therefore, it can be neglected in this analysis. Figure 6 also illustrates the electrostatic force involved in this simulation. F_3 and F_1 are forces towards BEAM1 in both directions, up and down, while F_2 is the force towards BEAM2. Physical dimension of this structure is given in Table 1. Si film for BEAM1 and BEAM2 must be as thin as possible in order to have a

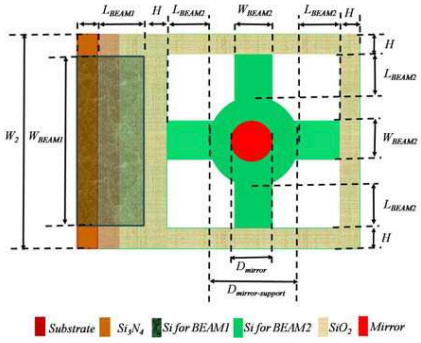

Figure 5. Layout of MEMS f-FPOTF.

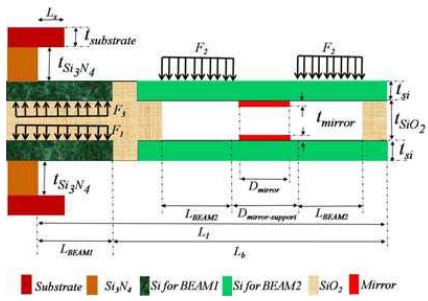

Figure 6. Cross-section of MEMS f-FPOTF.

Table 1. Dimension of MEMS f-FPOTF.

Parameter	**Value** (μm)
BEAM1	
$L_{BEAM\ 1}$	200
L_1	1000
L_b	800
L_s	20
$W_{BEAM\ 1}$	500
t_{Si3N4}	2
t_{si}	4.1
t_{SiO2}	0.9
BEAM2	
L_{BEAM2}	85
W_{BEAM2}	100
$D_{Mirror\text{-}suppor}$	330
t_{si}	4.1
$t_{spacer}=t_{SiO2}-2x(t_{mirror})$	0.6
Other dimension	
D_{Mirror}	125
t_{Mirror}	0.1
H	50
W	600

small value of DC voltage supply. However, in this design, Si film with 4.1 μm thickness is chosen since it is a challenge to have a floating FP cavity with very thin film.

In this paper, MEMS f-FPOTF is designed as a wavelength selector for CWDM application. Several aspects have to be considered in designing optical MEMS device. The main parameter is optical performance, especially in terms of transmissivity, tuning range and FWHM of the bandpass region. Since MEMS technology involves other engineering discipline, understanding of mechanic and electrostatic properties is useful for an optimal design.

3. ANALYSIS AND DISCUSSION

Analysis is divided into three main parts, optical, mechanic and electrostatic.

In optical analysis, MEMS f-FPOTF improvement on free spectral range (FSR) and how this design influences the FWHM and transmissivity of this filter are presented. As afore mentioned, CWDM application requires 360 nm tuning range. Thus, this filter needs a minimum 360 nm FSR to avoid overlapping between spectrums. The following section will discuss this matter.

Second analysis on mechanic will investigate the effect of beam displacement to mirror parallelism. This is very crucial since mirror parallelism will influence FPOTF finesse. Third part, which is the electrostatic analysis, will provide the expected operating voltage for each electrostatic cavity.

3.1. Optical Analysis

Analytical analysis on FPOTF transfer function is done to evaluate the performance in terms of tuning range, transmissivity and FWHM. Two simulation models which are conventional dual beam MEMS FPOTF and MEMS f-FPOTF have been developed using Matlab® mathematical software. Initial optical cavity for both models is 1.6 μm. Assuming pull in voltage for both models occurs at 1/3 of capacitance gap, and metallic mirror is used with Si film as a mirror support. Since maximum acceptance angle for CrAu in this structure is 8°, initial incident angle for MEMS f-FPOTF is set at 6°. Table 2 lists the parameters involved in this simulation.

Figures 7(a), 7(b), 8(a) and 8(b) show the relative intensity spectrum for minimum and maximum spectral for both simulation

Table 2. Optical analysis parameter setting.

Parameter	MEMS f-FPOTF	Dual Beam MEMS FPOTF
Max. deflection (Optical cavity)	$2 \times 0.533\,\mu m$	$2 \times 0.533\,\mu m$
Max. deflection (Electrostatic cavity)	$2 \times (\pm 2^\circ$ beam deflection)	None
Initial light incident angle (θ_0)	6°	0°
Refractive Index, n_2 (optical cavity)	1.0	1.0
Mirror reflectivity, R	95%	95%

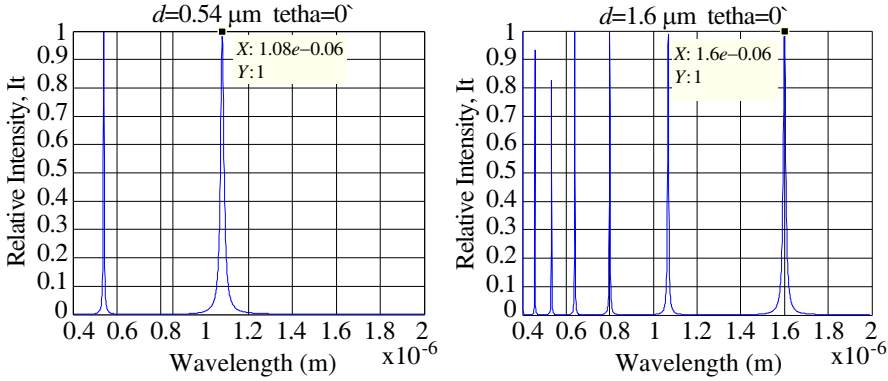

Figure 7. Conventional Dual Beam MEMS FPOTF minimum and maximum operating wavelength.

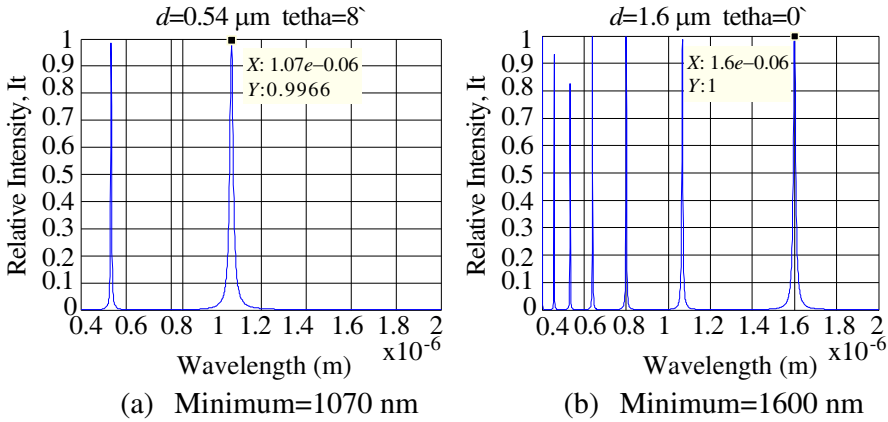

Figure 8. MEMS f-FPOTF minimum and maximum operating wavelength.

models. Both models give the same value of free spectral range (FSR) which is 540 nm. The tuning range of MEMS f-FPOTF, however, improves about 1.92% or 10 nm with respect to the conventional dual beam MEMS FPOTF. This is due to actuating floating cavity features on the proposed model. As a drawback, the relative peak intensity of MEMS f-FPOTF degrades about 0.01 in average while the FWHM expands about 5 nm greater than conventional MEMS FPOTF. MEMS f-FPOTF relative peak intensity and FWHM value however fulfilled the CWDM ITU-T G.694.2 standard.

3.2. Mechanic Beam Displacement Analysis

Deflection of BEAM1 in MEMS f-FPOTF would cause mirror tilting in optical floating cavity. To study this effect, finite element analysis (FEA) is developed. A range of 1×10^4 to 9×10^4 Pa pressure is applied on BEAM1 top surface located at bottom SOI wafer. Then, the displacement at the centre of FP mirror is analyzed.

Figure 9 shows the displacement on MEMS f-FPOTF structure due to 1×10^4 Pa pressure applied. Deflection of BEAM1 causes the FP cavity bent towards the bottom SOI substrate. Since there is no loading in region $L_{BEAM1} \leq x \leq L_b$ and free end boundary condition, this part will not bent but simply a straight line of slope. Therefore, the bent angle at the centre of mirror is equivalent to angle at point $x = L_{BEAM1}$. Figure 10 plots the deflection for both up and bottom mirrors. Both mirrors produce almost similar deflection. The difference is about 0.04% and shows a high parallelism between these two reflectors. As mentioned, high mirror parallelism will increase filter finesse.

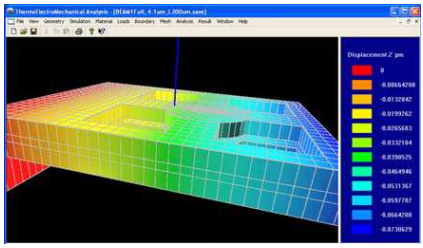

Figure 9. Displacement of MEMS f-FPOTF due to 1×10^4 Pa pressure applied on BEAM1.

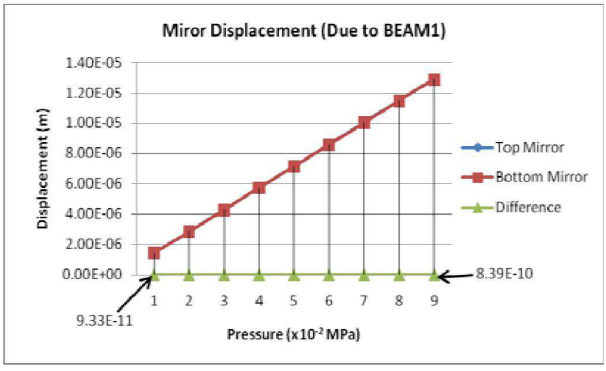

Figure 10. Displacement at the centre of MEMS f-FPOTF mirror.

3.3. Electrostatic Analysis

Operating voltages (V_1, V_2 and V_3) of the proposed structure is limited by pull in voltage, V_{pin} at each electrostatic cavity. In this analysis, pull in is assumed to occur at 1/3 of capacitance gap. Therefore, voltage at this point is considered as a V_{pin}.

FEA of electro-mechanic coupling analysis for BEAM1 is plotted in Figure 11. This is the operating voltage for V_1 and V_3. Thicker film needs higher voltage to deflect. As for BEAM1, about 500 volt is needed to deflect 3 nm of BEAM1 at $L = L_s$. 1 nm deflection of BEAM1 can shift about 1 nm MEMS f-FPOTF operating wavelength. The first prototype is expected to proof the principle of the proposed structure. Voltage for BEAM1 can be reduced by using thinner Si film.

Figure 12 gives the displacement of BEAM2 for a given V_2. Electrostatic force attracts these two beams, hence decreases the optical length of cavity, d. V_{pin} for this dual beam structure is about 33 Volt.

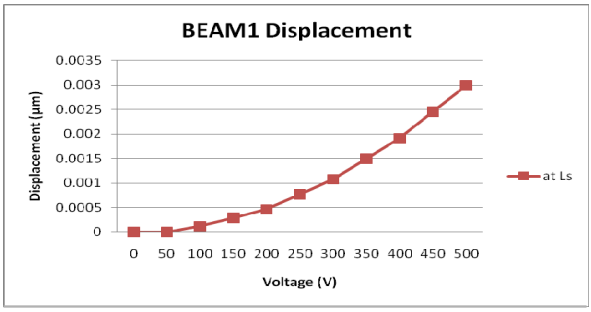

Figure 11. Displacement of BEAM1 MEMS f-FPOTF structure at $L = L_s$.

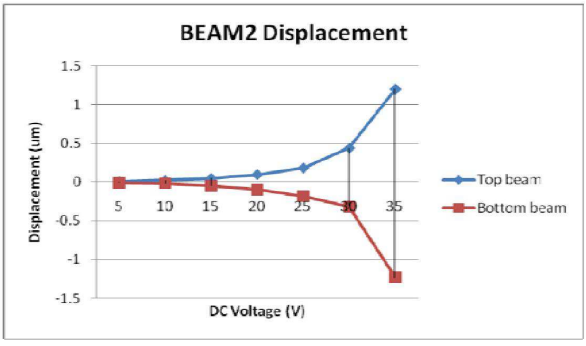

Figure 12. Displacement of BEAM2 MEMS f-FPOTF.

4. CONCLUSION

In conclusion, simulation model of MEMS f-FPOTF has been successfully developed to evaluate optical, mechanic and electrostatic behaviours. Analytical modelling shows that 1.92% or 10 nm improvement is achieved in terms of tuning range without sacrificing too much in the transmittivity. This enhancement adds one extra channel for CWDM application and 10 extra channels in DWDM ITU 100 GHz grid. Tuning range can be further improved by using DBR mirror, where higher initial angle can be set for this proposed device.

FEA simulation constructs pattern of mechanic beam displacement and its effect to mirror parallelism. Good parallelism between up and bottom mirrors in the proposed structure increases the filter finesse.

As for the electrostatic analysis, V_1 and V_3 consume high operating voltage to actuate BEAM1. This is a drawback of the proposed structure. Reducing thickness of SOI device layer will reduce the voltage. Fabrication aspect and experimental results will be discussed in the future in order to investigate the feasibility aspects of this proposed structure.

REFERENCES

1. Cheng, J., et al., "Analytical and finite element model pull-in study of rigid and deformable electrostatic microactuators," *Journal of Mechanics and Microengineering*, Vol. 14, IOP Publishing, 2004.
2. Robinson, K. C., "Single lense tunable wavelength division multiplexing Fabry Perot filter using MEMS technology," US 6,426,830 B1, Jul. 30, 2002.
3. Verma, R. K., et al., "Tunable Fabry Perot interferometer using entropic materials," US 6,597,461 B1, Jul. 22, 2003.
4. Chang, S. and S. C. Chang, "Fabry Perot optical filter device," US 6,700,706, US Patent, Mar. 2, 2004.
5. Little, M. J., "Detunable Fabry Perot interferometer and add/drop multiplexer using the same," US 2003/0123125 A1, Jul. 3, 2003.
6. Zhou, D. C. and S. J. Sheih, "Optical channel monitor using an angle tuned Fabry Perot optical filter," US 2003/0202799 A1, Oct. 30, 2003.
7. Chang, S. and C. Y. Juan, "Method for finesse compensation in a

Fabry Perot device and a Fabry Perot device with high finesse," US 2004/0100678 A1, May 27, 2004.

8. Verghese, P. M., "Dual membrane single cavity Fabry Perot MEMS filter," US 2005/0134962 A1, Jun. 23, 2005.
9. Kanbara, N., et al., "Precisely tunable Fabry-Perot filter for optical communications," *IEEE/LEOS International Conference on Optical MEMs*, 173–174, Aug. 2002.
10. Saadany, B., et al., "Free space tunable add drop optical filters using vertical bragg mirrors on silicon," *IEEE Journals of Selected Topics in Quantum Electronics*, Vol. 12, No. 6, Nov./Dec. 2006.
11. Ramam, A., et al., "MEMS tunable Fabry Perot optical filter," *IEEE/LEOS International Conference on Optical MEMS and Their Applications Conference*, 157–158, Aug. 1–4, 2005.
12. Halbritter, H., et al., "MEM tunable and wavelength selective receiver front end," *18th IEEE International Conference on Micro. Electro. Mechanical Systems*, 68–71, Jan. 30–Feb. 3, 2005.
13. Hohlfeld, D. and H. Zappe, "Micromachined tunable optical filters with optimized band pass spectrum," *The 12th International Conference on Solid Sensors, Actuators and Micro. Systems*, Boston, Jun. 8–12, 2003.
14. Keating, A. J., et al., "Optical characterization of Fabry Perot MEMS filters integrated on tunable short-wave IR detectors," *IEEE Photonics Technology Letters*, Vol. 8, No. 9, 2006.
15. Daleiden, J., et al., "Record wavelength tuning of 127 nm for vertical cavity Fabry-Perot filter," *IEEE/LEOS International Conference on Optical MEMs*, 169–170, Aug. 20–23, 2002.
16. Milne, J., et al., "Extended tuning range FP Etalon with doubly supported beam actuators," *IEEE/LEOS International Conference on Optical MEMS and Their Applications Conference*, 2006.
17. Chang, S. and C. H. Chang, "Method of manufacturing MEMS Fabry Perot devices," US 2004/0111856 A1, Jun. 17, 2004.
18. Madhumita, D., et al., "Design of MEMS tunable novel monolithic optical filters in InP with horizontal bragg mirrors," *Solid-State Electronics*, Vol. 48, 2004.
19. Yun, S. S., K. W. Jo, and J. H. Lee, "Crystalline Si-based in-plane tunable FP filter with wide tunable range," *International Conference on Optical MEMS*, 77–78, Aug. 2003.
20. Huang, H., et al., "Mechanical design and finite element modelling of tunable Fabry Perot MEMS structure for adaptive infrared detectors," *IEEE Conference on Optoelectron. and Microelectron*

Mat. and Dev., Australia, Dec. 8–10, 2004.

21. Bazu, M., et al., "Reliability assessment by virtual prototyping of MEMS tunable Fabry-Perot optical cavity," *2004 International Semiconductor Conference, CAS 2004 Proceedings*, Vol. 1, Oct. 4–6, 2004.
22. Flanders, D. C., P. S. Whitney, and M. F. Miller, "Flexible membrane for tunable Fabry-Perot filter," US 6,341,039 B1 US Patent, Jan. 22, 2002.
23. Meissner, P., et al., "Micromachined two chips filters for WDM transmission system," *2002 IEEE/LEOS International Conference on Optical MEMs*, 167–168, Aug. 20–23, 2002.
24. Tucker, R. S. and W. V. Sorin, "Tunable Fabry-Perot filters and lasers," US 6,400,738 B1 Jun. 4, 2002.
25. Tucker, R. S. and W. V. Sorin, "Optically tunable Fabry-Perot microelectromechanical resonator," US 6,714,565 B1, US Patent, Mar. 30, 2004.
26. Taebati, P., et al., "Microelectromechanically tunable, confocal, vertical cavity surface emitting laser and Fabry Perot filter," US 2002/0031155 A1, US Patent, Mar. 14, 2002.
27. Halbritter, H., et al., "Impact of micro. mechanics on the linewidth and chirp performance of MEMS VCSEL," *IEEE Journals of Selected Topics in Quantum Electronics*, Vol. 13, No. 2, Mar./Apr. 2007.
28. Flanders, D. C., "Dual cavity MEMS tunable Fabry Perot filter," US 6,424,466 B1 US Patent, Jul. 23, 2002.
29. Cook, C. C., "Dual band Fabry Perot mirror coating," US 2002/0181107 A1, US Patent, Dec. 5, 2002.
30. Lu, L. J., "Tunable Fabry Perot filter," US 2004/0218865, Nov. 4, 2004.
31. Atia, W. A., et al., "MEMS Fabry-Perot filter for integrated spectroscopy system," US 2006/0197958, Sep. 7, 2006.
32. Iizuka, K., *Elements of Photonics*, John Wiley & Sons, Inc, 2002.
33. Ugural, A. C., *Mechanical Design: An Integrated Approach*, Mc Graw Hill, 2004.
34. Ngajikin, N. H., et al., "FEM simulation on MEMS FPOTF using aluminum metallic mirror," *IEEE Fourth International Conference on Wireless and Optical Communication Networks*, 2008.
35. Ngajikin, N. H., et al., "Modelling of MEMS FP OTF for wavelength tuning in CWDM application," *IEEE International Conference on MEMS and Nanotechnology*, 2008.
36. Anderson, D. E. and A. L. V. Brocklin, "Fabry Perot

interferometer," US 7,061,681 B2, Jun. 13, 2006.

37. Missey, et al., "Microelectromechanical tunable Fabry-Perot wavelength monitor with thermal actuators," US 2003/0053078 A1, Mar. 20, 2003.
38. Spiegelberg, C. P., et al., "Erbium doped phosphate glass tunable single mode fiber laser using tunable Fabry Perot filter," US 2004/0196874 A1, Oct. 7, 2004.
39. Hohlfeld, D., M. Epmeier, and H. Zappe, "Tunable thermo optic. filter for WDM applications," *The Fifteenth IEEE International Conference on Micro. Electro. Mechanical Systems*, 2002.
40. Marty, F., et al., "High aspect ratio nano structures (HARNS) for photonic MEMs based on vertical DBR architecture," *The 13th International Conference on Solid Sensors, Actuators and Micro. Systems*, Korea, Jun. 5–9, 2005.
41. Nakagawa, W. and Y. Fainman, "Tunable optical nanocavity based on modulation of near field coupling between sub-wavelength periodic nanostructure," *IEEE Journals of Selected Topics in Quantum Electronics*, Vol. 10, No. 3, May/Jun. 2004.
42. Tucker, R. S., et al., "Tunable Fabry Perot filters and lasers using feedback to reduce frequency noise," US 6,538,748 B1, US Patent, Mar. 25, 2003.
43. Tucker, R. S. and W. V. Sorin, "Tunable Fabry Perot filters and lasers using feedback to reduce frequency noise," US 6,724,785 B1, US Patent, Apr. 20, 2004.
44. Tucker, R. S., et al., "Thermal noise and radiation pressure in MEMs Fabry Perot tunable filters and lasers," *IEEE Journal on Selected Topics on Quantum Electronics*, Vol. 8, No. 1, Jan./Feb. 2002.
45. Chang, S., "Fabry Perot device compensating for an error of full width at half maximum and method of making the same," US 2004/0075845 A1, Apr. 2, 2004.
46. Bao, Y., "Waferless fiber Fabry-Perot filters," US 2004/0247244 A1, Dec. 9, 2004.